General Disclaimer

One or more of the Following Statements may affect this Document

- This document has been reproduced from the best copy furnished by the organizational source. It is being released in the interest of making available as much information as possible.

- This document may contain data, which exceeds the sheet parameters. It was furnished in this condition by the organizational source and is the best copy available.

- This document may contain tone-on-tone or color graphs, charts and/or pictures, which have been reproduced in black and white.

- This document is paginated as submitted by the original source.

- Portions of this document are not fully legible due to the historical nature of some of the material. However, it is the best reproduction available from the original submission.
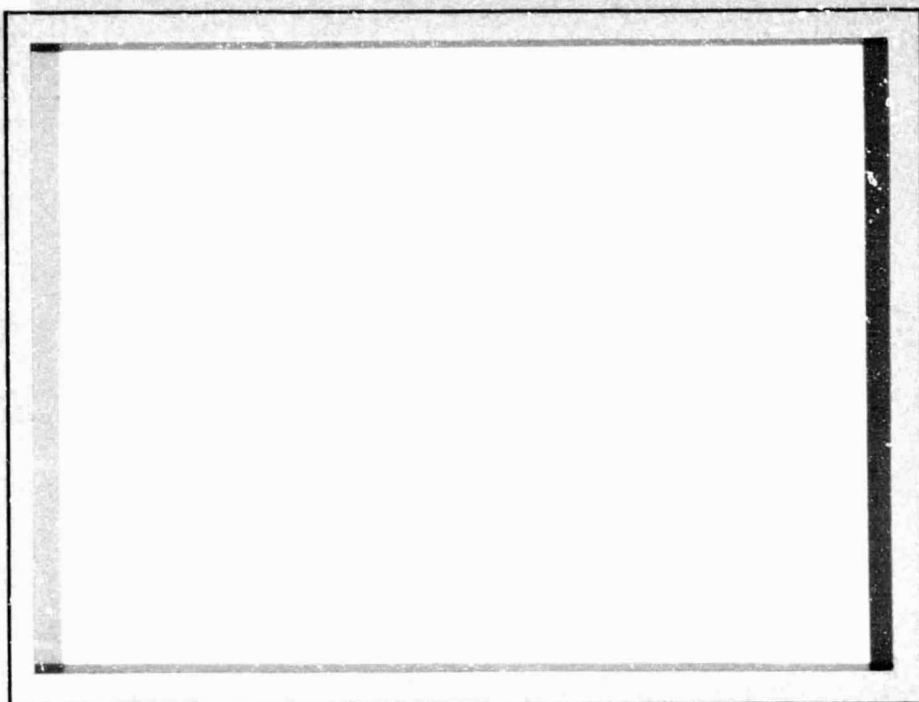
C S S A

CENTER FOR SPACE SCIENCE AND ASTROPHYSICS
STANFORD UNIVERSITY
Stanford, California

THE DEVELOPMENT AND TEST OF ULTRA-LARGE-FORMAT

MULTI-ANODE MICROCHANNEL ARRAY DETECTOR SYSTEMS

Progress Report for NASA Grant NAGW-551
for the period 1 June through 30 November 1984

J. G. Timothy
Principal Investigator

Center for Space Science and Astrophysics
Stanford University
Stanford, California 94305

INTRCDUCTION

During the past six months, significant progress was made with all aspects of the detector system development. Indeed, a major program milestone was reached in that quantitative data were recorded showing that we can now fully define the detector system configurations that are needed for use in both sealed configurations at ultraviolet and visible wavelengths and in open-structure configurations at extreme-ultraviolet (EUV) and soft x-ray wavelengths. The specific tasks that were accomplished with each of the key elements of the detector system are described in the following sections of this report.

HIGH-GAIN MICROCHANNEL PLATES

The problem that has delayed this program for almost a year, specifically the lack of adequate curvature in the channels of the high-gain MCPs fabricated by Galileo Electro-Optics, has finally been overcome. We have now received a number of units of the curved-channel MCPs with 12-micron channel diameters and channel length-to-diameter ratios in the range from 100-140:1. The performance characteristics of these MCPs are excellent and display none of the problems of ion feedback observed with units delivered during the second half of 1983. As an example of the type of output pulse-height distribution being obtained, the distribution for a curved-channel MCP with 12-micron, 100:1 length-to-diameter ratio channels operated in a sealed ultraviolet detector tube is shown in Figure 1. The modal gain of this MCP is 1.1×10^6 electrons pulse^{-1}, and the resolution of the output pulse-height distribution is 45%.

We have also implemented a number of changes to the MCP structure in order to optimize the performance in the sealed ultraviolet and visible-light detector tubes. First, a 50 A-thick, SiO_2 ion-barrier membrane is deposited on
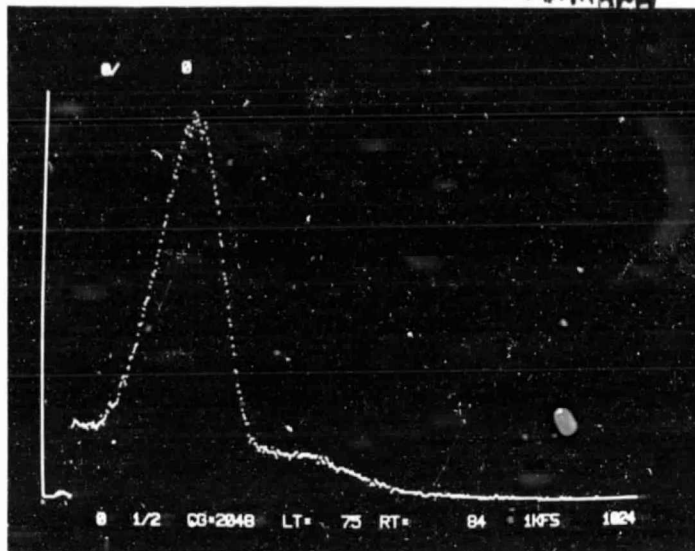
1

Figure 1. Output pulse-height distribution for a curved-channel MCP with 12-micron-diameter channels. Modal gain 1.1×10^6 electrons pulse^{-1}, resolution (FWHM) 45%.

the front face of the MCP. This has been found to be necessary in order to prevent the feedback of ions from the MCP channels to the proximity focussed, semi-transparent photocathode. This feedback causes afterpulses which are recognized by the MAMA detector system electronics as invalid events (lowering the detective quantum efficiency) and over a long period of time causes a significant degradation in the photocathode quantum efficiency. We have also added a thin coating of MgO on the front face of the MCP under the SiO_2 ion-barrier membrane in order both to enhance the gain and to reduce the reflection of photons back to the semi-transparent photocathode which can degrade the point-spread function. Tests of the first MgO-coated, curved-channel MCP are about to begin.

Construction of an ultra-high vacuum system designed specifically for bake and "scrub" studies of high-gain MCPs with diameters of up to 100 mm has now been started. The system will be ready for initial MCP tests at the end of January.

PHOTOCATHODES

We have continued to fabricate sealed ultraviolet and visible-light MAMA detector tubes at Litton Electron Devices using the tube structure shown in Figure 2. The quantum efficiencies of these photocathodes are shown in Figure 3, and some details of the MCP tube characteristics are given in the
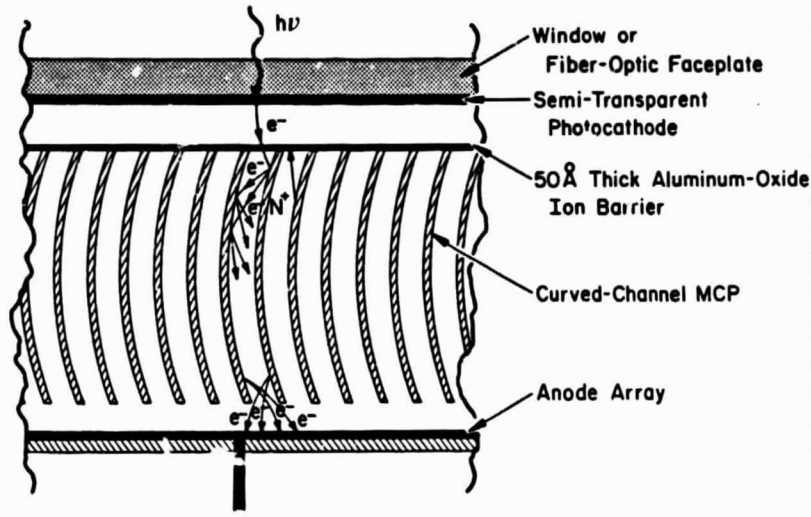

Figure 2.   Schematic of MAMA detector tube with proximity-focused, semi-transparent photocathode.
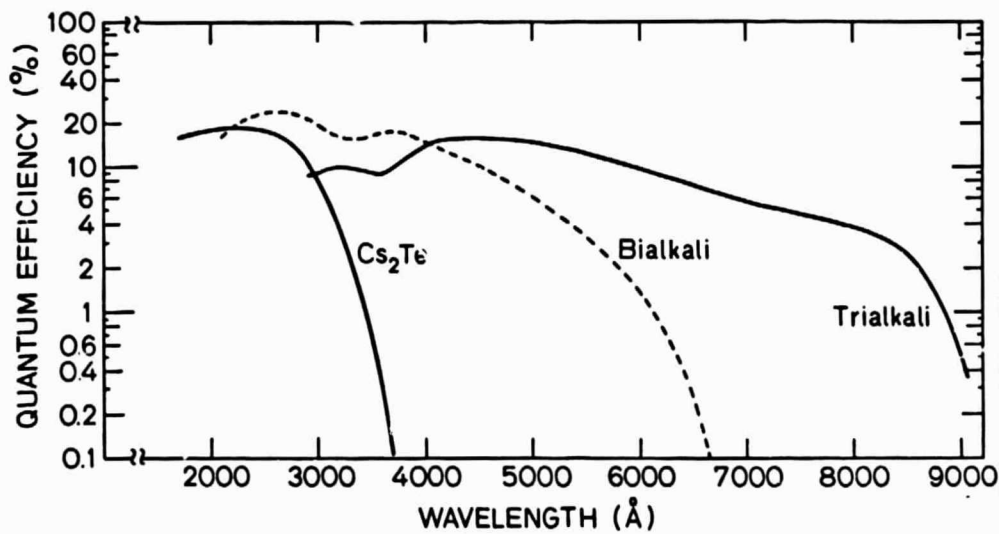

Figure 3.   Quantum efficiencies of semi-transparent ultraviolet and visible-light photocathodes in the MAMA detector tubes.

reprint attached to this report. Most importantly, not only are we obtaining high cathode quantum efficiencies, but we are now also obtaining high detective quantum efficiencies in the pulse-counting mode. Detective quantum efficiencies ranging from 65-80% of the photocathode quantum efficiency have so far been obtained for the different array configurations. Detailed measurements of the overall transfer efficiencies of the imaging detector tubes are now in progress.

ANODE ARRAYS

The evaluations of the (1 x 1024)-, (16 x 1024)-, and (256 x 1024)-pixel, coincidence-anode arrays have shown that these arrays, constructed solely with conducting electrodes, provide a high detective quantum efficiency in the pulse-counting mode. However, a number of highly significant results have been obtained as a result of the test program during the past six months. One of the key findings is that the signal-to-noise measured at the inputs of the amplifiers is lower than expected by at least a factor of two and probably a factor of three. Since the charge cloud from the MCP is divided a maximum of six ways in the MAMA readout array, this has no significant impact on the ability of the MAMA detector system to operate with a high detective quantum efficiency and a low background in the space environment. It does, however, emphasize the need for using amplifier and discriminator circuits with thresholds in the range 5×10^4 to 1×10^5 electrons pulse^{-1} even when the modal gain of the MCP is in excess of 10^6 electrons pulse^{-1}. We believe that this loss of signal is probably being caused by some inductive coupling effect in the electrode structure. Since the charge pulse leaving the high-gain MCP is extremely narrow (pulse width of the order of, or less than, 300 ps), inductive effects may well become significant in the anode array electrode structure at these

effective frequencies in excess of 3 GHz. This finding has significant effects on the operation of more complex readout arrays such as the Codacon where the signal-to-noise is reduced further by the use of a capacitively coupled electrode structure and where the charge is divided between ten or more electrodes. Another effect that has now been quantified is the fixed pattern observed in the raw flat-field response of the MAMA detectors as shown in Figure 4. It can be seen that there is a periodic pattern which damps out for 4 out of every 64 pixels. This, it is now clear, is caused by coupling between the coarse-encoding electrodes in the present anode array structure. As the anode array is presently configured, the coarse electrodes in the decode area can only couple to each other, while each fine electrode couples signal to all of the other 31 fine electrodes. It should be noted that this fixed pattern is extremely stable with both time and signal level and rectifies with an accuracy equal to the photon statistics as shown in Figure 4. Further, Fourier transform analyses of rectified images show no power. However, this fixed pattern is cosmetically unattractive, and careful analysis of the data show that this preferential coupling is invalidating a number of detected events at about the 2% level. In order to provide the maximum uniformity of response and the maximum detective quantum efficiency, we have accordingly reconfigured the encoding electrodes of the anode array in order to lower the total capacitance and to balance the coupling of the coarse- and fine-encoding electrodes. The first modified array with a (1 x 1024)-pixel configuration is now ready for quantitative study which hopefully will be completed by the end of February 1985. Following this analysis, we plan to reconfigure the (256 x 1024)-pixel array prior to proceeding with the fabrication of the (1024 x 1024)-pixel array.
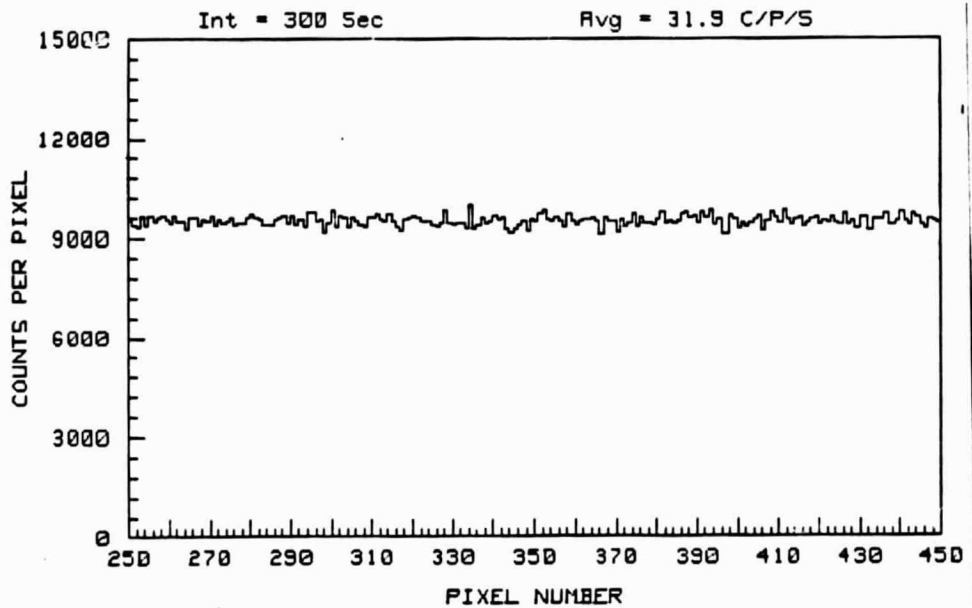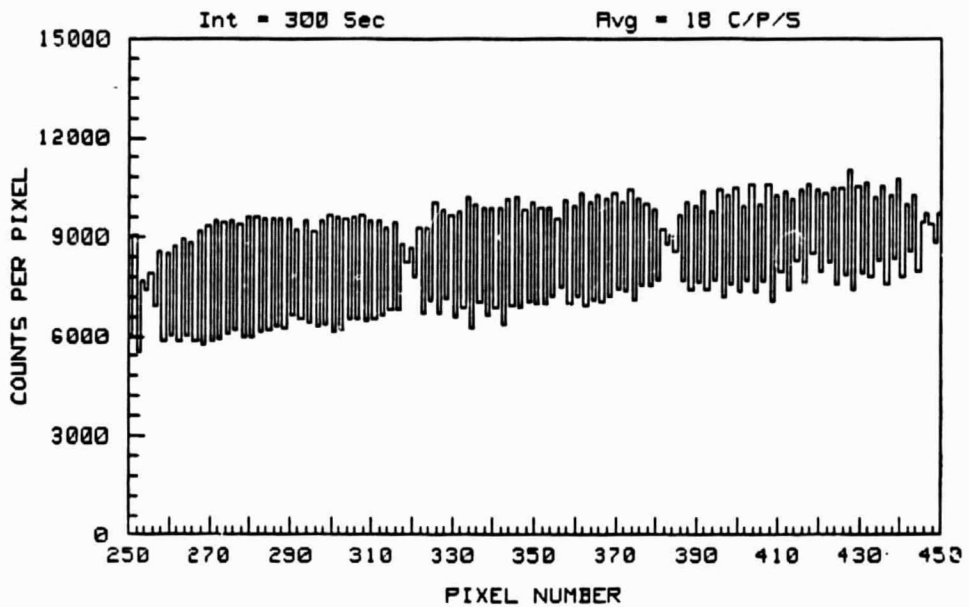
Figure 4. Upper: Raw flat field for one axis of a (256 x 1024)-pixel
MAMA detector.
Lower: Rectified flat field for one axis of a (256 x 1024)-
pixel MAMA detector.

6

ELECTRONICS

As described in the previous sections, it has been determined that new amplifier and discriminator circuits with thresholds of the order of 5×10^4 electrons pulse^{-1} will be required for the high-resolution imaging detector systems. Accordingly, we are initiating the design of a new amplifier circuit board which can accommodate ten Amptek, Inc., A-111 amplifier and discriminator circuits in hybrid form. The first of these boards should be completed and ready for test during the first half of 1985. It is expected that the combination of these boards and the reconfigured anode arrays will provide the definitive system which will provide the maximum sensitivity and stability for flight operation in both the open-structure and sealed configurations.

ATTACHMENTS

"Performance Characteristics of Multi-Anode Microchannel Array Detector Systems," by J. G. Timothy.

"Electronic Readout Systems for Microchannel Plates," by J. G. Timothy

Performance characteristics of multi-anode microchannel array detector systems

J. G. Timothy

Center for Space Science and Astrophysics, Stanford University
ERL 315, Stanford, California 94305

Abstract

Multi-anode microchannel array detector systems with formats as large as 256 x 1024 pixels are currently under evaluation in the laboratory. Preliminary performance data for sealed ultraviolet and visible-light detector tubes have shown that the detector systems have unique characteristics which make them complementary to photoconductive array detectors, such as CCDs, and superior to alternative pulse-counting detector systems employing high-gain MCPs.

Introduction

The multi-anode microchannel arrays (MAMAs) are state-of-the-art, pulse-counting, photoelectric array detectors designed specifically for use in space astrophysics instruments. The construction and modes of operation of the different MAMA detector systems have been described earlier[1,2,3] and will not be reviewed in detail here. In this paper recent progress with the development of ultraviolet and visible-light versions of the MAMA detectors will be described and their operating characteristics compared and contrasted with those of photoconductive array detectors, such as the CCDs. Preliminary performance data for MAMA detectors with formats as large as 256 x 1024 pixels will be presented and the goals of the the development program summarized.

MAMA Detector System Design Parameters

The MAMA detectors have been designed from the outset to provide the spatial resolution and dynamic range required for high-resolution imaging and spectroscopy, a noise level set solely by the photon statistics and the photocathode dark current, and to operate with maximum reliability in the space environment. In order to meet these requirements, the MAMA detector system uses a minimum number of components in the detector tube and conservatively rated, low-power electronics.

The components of a MAMA detector tube consist of a sealed or open-structure tube assembly containing a single high-gain, curved-channel microchannel plate (MCP) intensifier stage with an appropriate photocathode material deposited on or mounted in proximity focus with the front face. A set of anode electrodes of the appropriate configuration is mounted in proximity focus with the output face of the MCP and is used to uniquely identify the position of the detected photon event. Two different types of multi-anode arrays have been developed. The discrete-anode array employs a charge amplifier and discriminator circuit connected to each anode, i.e. pixel, and provides a very high dynamic range but only a limited number of pixels ($\lesssim$ 500). Output pulses from the MCP that exceed a preset charge threshold are accumulated in external counting circuits for a predetermined exposure time controlled by an electronic shutter signal. The number of events recorded in each counting circuit is proportional to the number of photons incident upon that part of the photocathode on the front face of the MCP that corresponds spatially to the anode location.

The coincidence-anode array which employs sets of two or more electrodes in a multilayer structure (see Figure 1) to detect the charge pulse from the MCP, provides the very large number of pixels required for high-resolution imaging applications (10^5 to 10^6 pixels) with a practical number of amplifier and discriminator circuits and with some limitations on the dynamic range. Again, the detector pixels are defined by the dimensions of the sets of anode electrodes. A charge amplifier and discriminator circuit which issues a logic pulse for each output pulse from the MCP that exceeds a preset charge threshold is connected to each set of anode electrodes. Any valid combination of coincident logic pulses is decoded to determine the spatial location of an event, and the number of events occurring at each location is stored in the corresponding word of a random access memory (RAM). Alternatively, the address of each detected event can be stored on an external recording medium such as magnetic tape.

Both the discrete-anode and coincidence-anode MAMA detectors are random readout systems with the detected events stored in an external memory. It is accordingly possible to determine not only the physical location of the detected event, but also its arrival time with an accuracy equal to the pulse-pair resolution of the electronic circuits.
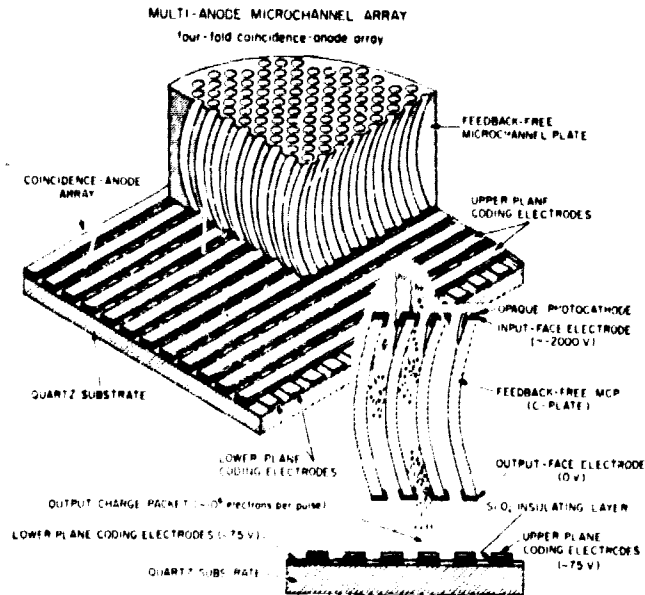
MULTI-ANODE MICROCHANNEL ARRAY
four-fold coincidence-anode array

Figure 1. Schematic of MAMA detector tube with multi-layer coincidence-anode array.

Operating Characteristics of MAMAs and CCDs

A range of photoemissive and photoconductive array detectors with high sensitivities and high-resolution imaging capabilities are now becoming available as the result of both the meteoric expansion of the semiconductor industry and the continuing emphasis on the development of low-light-level imaging systems for military and civilian surveillance applications. In particular, photoconductive array detectors, such as the Charged-Coupled Devices (CCDs), are becoming widely used for astronomical studies because of the very high intrinsic quantum efficiencies of silicon at red and near-infrared wavelengths and because of their geometric fidelity and low readout noise.[3] There are, however, a number of limitations in the operating characteristics of the CCDs which are not present in photoemissive detectors and the MAMAs accordingly represent a powerful complementary capability for astrophysical investigations. First, the CCDs integrate charge on the chip and use a serial readout technique. For this reason, they are not suitable for applications which require fast timing of events such as speckle imaging or speckle spectroscopy. In comparison with the CCDs, the MAMAs use a random readout system, and events can be time-tagged to an accuracy equal to the pulse-pair resolution of the electronics. CCDs operate with unity gain and have a finite readout noise. The MAMAs are pulse-counting detectors with gains of the order 10^5 to 10^6 and operate with zero readout noise. Potentially the MAMAs can provide a better signal-to-noise than the CCDs at low light levels although this advantage is at present offset by the low quantum efficiencies of photoemissive cathodes at red and near-infrared wavelengths. UV flooding of CCDs has now allowed them to operate with high efficiency down to blue and near-ultraviolet wavelengths. However, photoemissive detectors, such as the MAMAs, have comparable or superior detection efficiencies at ultraviolet wavelengths. In addition, since the MAMAs use photoemissive cathodes, the sensitivity can be tailored to match the spectral range of interest, and ultraviolet versions can be made insensitive to longer wavelength radiation. CCDs have a very broad wavelength response with the peak sensitivity in the red. This can cause serious problems with scattered light for studies of objects with low levels of emission at ultraviolet wavelengths. CCDs require cooling to temperatures below -100°C for low-noise operation. The high-gain MCPs require no cooling for pulse-counting operation. Accordingly, only the visible-light MAMA detector tubes require cooling to temperatures in the range 0 to -30°C to reduce the thermionic emission from the photocathode. Finally, CCDs are sensitive to the cosmic ray background, an effect which is essentially unobservable with the MAMA detector tubes. The principal differences between the operating characteristics of the CCDs and the MAMAs are summarized in Table 1.

The prospects for future developments are also worth consideration. High-gain MCPs are already available with active areas significantly larger than those of the largest CCDs available today. In addition, preparations for the fabrication of high-gain MCPs with active areas greater than 100 mm in diameter are well advanced. The prospects for large-format CCDs are more obscure. Relatively little progress has been made with large single chips, and the availability of arrays of buttable CCDs seems unlikely in the near future.

Table 1. Comparison of MAMA and CCD Operating Characteristics

Parameter	MAMA	CCD
Signal Integration	In external memory	On chip
Gain	10^5 to 10^6	1
Pulse-Counting	Yes	No
Readout Noise	zero	$\gtrsim$ 10 electrons rms
Event Timing Accuracy	$\sim$ 100 ns	> 1 s for low-noise operation
Wavelength Response	Relatively narrow--tailored by photocathode material	Broad
Sensitivity	Ultraviolet - high Blue - moderate Red - low	Ultraviolet - low Blue - high Red - very high
Cooling Requirements	Ultraviolet photocathodes --none Visible-light photocathodes --0 to -30°C	Below -100°C for low-noise operation
Sensitivity to Cosmic Rays	Low	High--thick chips Moderate--thinned chips
Largest Active Area	7 x 27 mm^2	12 x 12 mm^2

MAMA Performance Characteristics

Ultraviolet and visible-light MAMA detector tubes that employ semi-transparent photocathodes as shown in the schematic in Figure 2, have recently been fabricated for the first time. The 25-mm-format sealed MAMA detector tube fabricated by Litton Electron Devices[4] which can accommodate arrays of up to 256 x 1024 pixels is shown in Figure 3. To date,
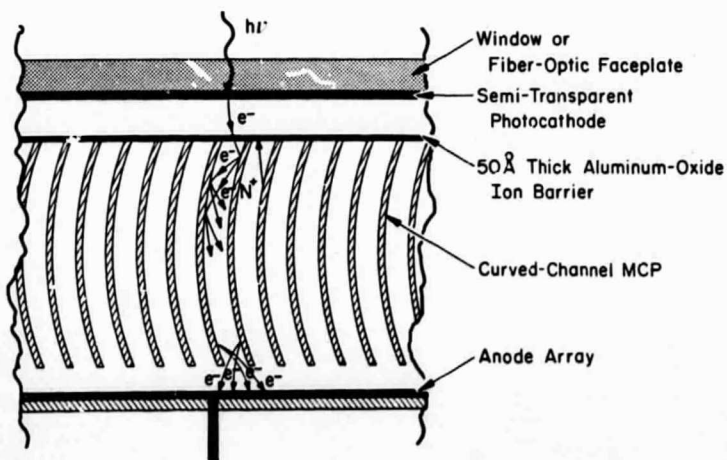

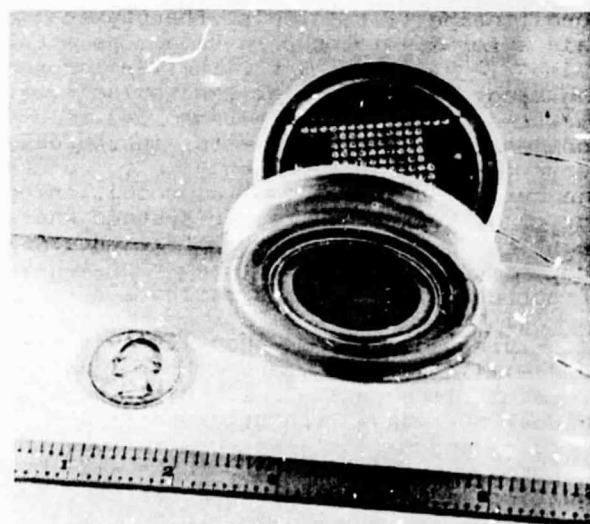Figure 2. Schematic of MAMA detector tube with proximity-focused, semi-transparent photocathode.

Figure 3. Sealed 25-mm-format MAMA detector tube.

a number of tubes with Cs_2Te ultraviolet and bialkali and trialkali visible-light photo-cathodes have been fabricated. Typical quantum efficiencies for these photocathodes are shown in Figure 4.
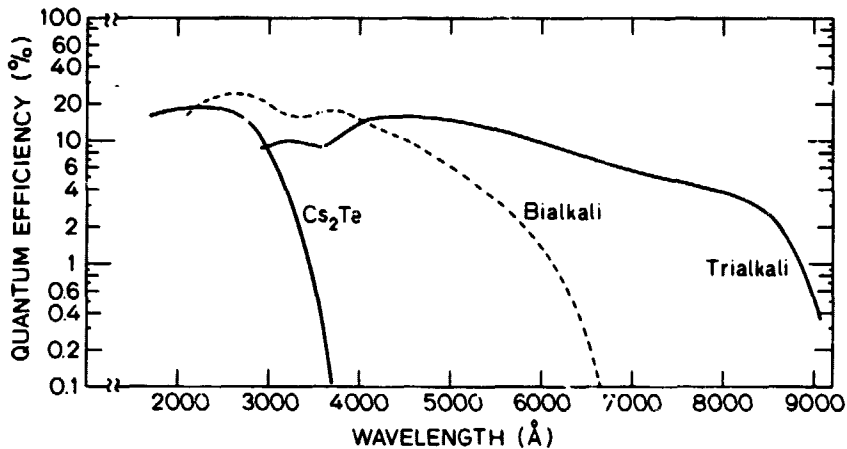

Figure 4. Quantum efficiencies of semi-transparent ultraviolet and visible-light photocathodes in the MAMA detector tubes.

One of the most important aspects of the sealed detector tube fabrication is the appropriate conditioning of the high-gain, curved-channel MCP by means of bake and scrub procedures. For the curved-channel MCPs supplied to date, fabricated by Galileo Electro-Optics[5] or by Litton Electron Devices, a bake at temperatures in excess of 300°C for periods well in excess of 48 hours is required to completely desorb the internal surface area and arrive at a pressure asymptote. Following this, a scrub by stimulating the MCP with either 600 eV electrons or with UV radiation from a mercury penray lamp is required to further clean up the internal surfaces and to reach a stable gain plateau. The scrub procedure consists of operating the MCP in a hydrocarbon-free, high-vacuum environment at progressively increasing values of the applied potential, and therefore the gain, and progessively increasing signal levels. Typically a total charge throughput of the order of or greater than 0.2 C cm^{-2} is required to reach a stable gain plateau. After conditioning, a stable response to an accumulated signal level of greater than 2.5×10^{11} counts mm^{-2} has so far been demonstrated.

It is important to note in this context that the gain of the curved-channel MCP after conditioning is related to the physical dimensions of the channels. Typical modal gain values for 25-micron-pore-size MCPs after scrub lie in the range from $1-3 \times 10^6$ electrons $pulse^{-1}$. Modal gains for the 12-micron-pore-size MCPs are proportionally lower and lie in the range $3-6 \times 10^5$ electrons $pulse^{-1}$. A single sample of an 8-micron-pore-size MCP has shown modal gains in the range $1-3 \times 10^5$ electrons $pulse^{-1}$. These values must be carefully considered as a key parameter in the design of any electronic readout system if a high detective quantum efficiency is to be attained. The output pulse-height distribution from the curved-channel MCP after conditioning is extremely narrow (see Figure 5) and is ideal for pulse-counting detector systems where a high photometric accuracy is required. Pulse-counting detective quantum efficiencies have been measured to be between 65 and 80% of the photocathode quantum efficiency at a given wavelength for MAMA detector tubes with this form of output pulse-height distribution.

Three coincidence-anode array formats are currently under evaluation; namely, the (1 x 1024)-, (16 x 1024)-, and (256 x 1024)-pixel systems. The basic parameters of these systems are summarized in Table 2. Over the active areas of 6.5 x 26 mm^2 of these arrays, curved-channel MCPs have been obtained with no bright emission points and with only a few dark spots caused by small defects in the structure of the channel bundles. It is our expectation that the number of these defects will be significantly reduced in the future as a result of modifications to the fabrication procedures now being undertaken at Galileo Electro-Optics.

The multi-layer anode structure requires precision fabrication techniques, and some concerns have been expressed about the feasibility of fabricating these structures. However, to date, defect-free versions of all three arrays have been fabricated, and recent improvements in the fabrication facility at Ball Aerospace Systems Division,[6] and the continuing development of the fabrication procedures have significantly improved the quality and yield of the (256 x 1024)-pixel arrays. The MAMA anode structure consists solely of conducting electrodes separated by insulators. It is accordingly extremely easy to identify defects
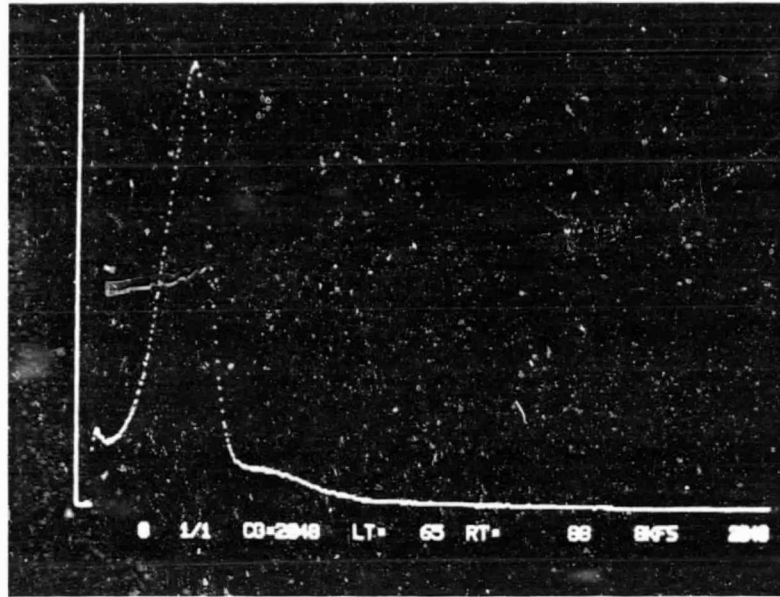
Figure 5. Output pulse-height distribution for curved-channel MCP with 25-micron-diameter channels. Modal gain 1.3×10^6 electrons pulse^{-1}. Resolution (FWHM) 40%.

Table 2. Characteristics of Coincidence-Anode Arrays

Format	Pixel Dimensions	Active Area	Number of Amplifiers
1 x 1024	6.5 mm x 25.4 microns	6.5 x 26 mm^2	64
16 x 1024	380 x 25.4 microns^2	6.5 x 26 mm^2	80
256 x 1024	25.4 x 25.4 microns^2	6.5 x 26 mm^2	96

during the fabrication process by either optical or electronic techniques. A number of defect-free anode arrays are now in hand and are being used for the fabrication of a series of detector tubes.

The anode array structure must be capable of surviving the environmental conditions within the detector tube. It has now been verified that the anode arrays can survive bake under vacuum at temperatures in excess of 300°C for the time periods required for the processing of the ultraviolet and visible-light sealed detector tubes. Further, provided that the MCP is properly conditioned and is not contaminated, no evidence for any degradation or damage to the anode structure as the result of extended tube operation has been observed.

One of the highly desirable features of the MAMA detector system is the absolute geometric fidelity resulting from the use of a proximity-focused system. Further, since no centroiding or analog interpolation techniques are employed for the identification of the location of the photon event, the image quality is independent of the signal level and is highly stable over long periods of time.[7] The geometric precision of the detector system, since a number of MCP channels are associated with each pixel, is simply the precision of the pattern-generating machine used for the fabrication of the anode array electrode structure. Measurements of both one- and two-dimensional readout arrays have shown geometric fidelity on the order of a few microns over distances of 26 mm. An image recorded with a (256 x 1024)-pixel ultraviolet MAMA detector tube which has been flat-field corrected but not geometrically rectified is shown in Figure 6. The geometric fidelty of the image is readily apparent together with the fact the detector is imaging at close to single-pixel response. This resolution of ~ 25 microns FWHM is superior to that of any other electronic MCP detector system that has so far been reported in the literature. The uniformity of the flat field response over the active area is of the order of or better than 25% peak-to-peak.
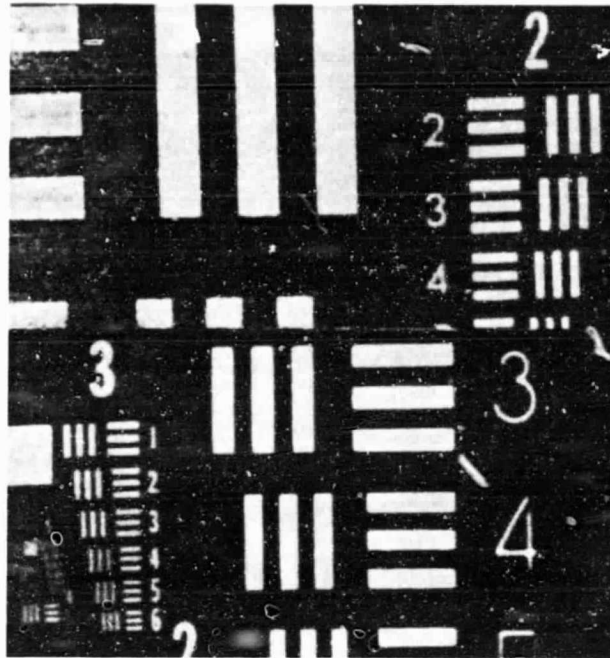
Figure 6. Ultraviolet image recorded with a (256 x 1024)-pixel MAMA detector system. Left half of image is at the top and right half of image is at the bottom. Bar pattern at lower left is of the order of 1-2 pixels wide.

The dynamic range of the MAMA detectors is set by two limitations; first, the maximum count rate capability per unit area set by the conductivity of the curved-channel MCP and second, the maximum total array count rate set by the pulse-pair resolution of the amplifiers, discriminators, and address decoding and RAM circuits. Curved-channel MCPs already in hand have demonstrated the capability to provide count rates in excess of 10^5 counts mm^{-2} s^{-1} (random) with a gain loss which is sufficiently low that the detective quantum efficiency is reduced by less than 10%. In the design of the MAMA electronics, there is complete flexibility in a tradeoff between speed and power, and as low-power monolithic circuits become increasingly available, the speed capabilities of the MAMA detector system will be significantly increased without any changes in the basic system design. At the present time, two low-power (256 x 1024)-pixel systems are in operation. The first, with a pulse-pair resolution of 800 ns, provides a total array count rate of about 1.2×10^5 counts s^{-1} (random) with a coincidence loss of less than 10%; and the second, with a pulse-pair resolution of 100 ns, provides a total array count rate of 10^6 counts s^{-1} (random) with a coincidence loss of 10%. The power requirements of these systems are summarized in Table 3. As well as requiring low power, the MAMA detector system is extremely compact. A complete (256 x 1024)-pixel system for flight on the Balloon-Borne Ultraviolet Stellar Spectrograph (BUSS) is shown in Figure 7. Correct operation of this system has been verified over the temperature range -30 to +30°C at an ambient pressure of 2 Torr.

Table 3. Power Requirements for the (256 x 1024)-pixel MAMA Dete tor Systems

Pulse-pair Resolution (ns)	Regulated Power (W)		
	Amplifiers and Discriminators (96)	Decoding Circuits and Random Access Memory	Computer Interface
800	2.5	16.5	3
100	7.7	16.5	3

Future Developments

Detailed measurements of the MAMA detector system performance characteristics are now in progress, and additional refinements of the (256 x 1024)-pixel detectors have been initiated. In particular, the anode array geometry has been slightly modified in order to improve the uniformity of response and increase the charge collection efficiency. Following
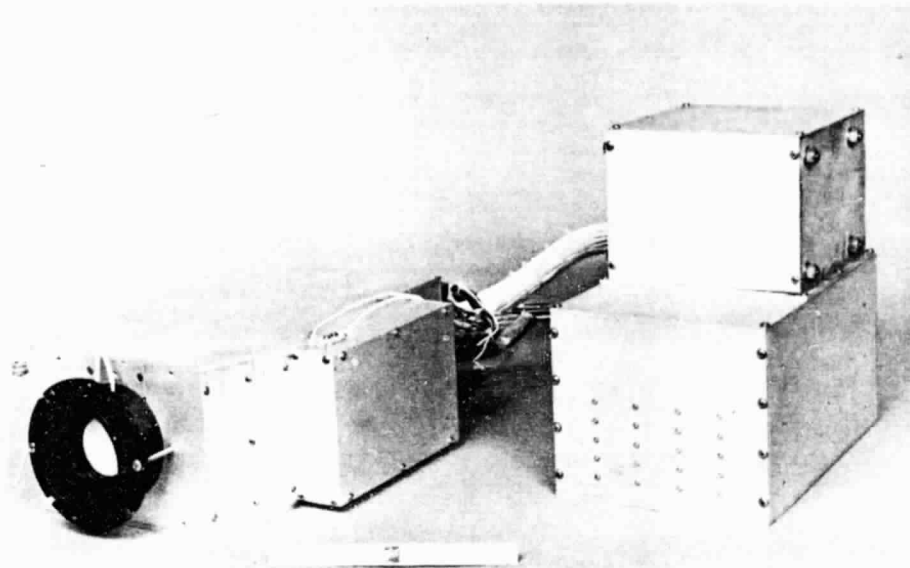
Figure 7. (256 x 1024)-pixel MAMA detector system for flight on the BUSS.

completion of these new arrays, a (1024 x 1024)-pixel array will be fabricated. 40-mm-format, curved-channel MCPs with square active areas of $27 \times 27 \text{ mm}^2$ to match this array (see Figure 8) are already in hand. Completion of this array is now expected early in 1985. 75-mm-format, curved-channel MCPs have just been fabricated for the first time by Galileo Electro-Optics, and the fixturing for curved-channel MCPs with active areas greater than 100 mm in diameter is currently under construction. The MAMA detector formats which can be accommodated within the active areas of these MCPs are shown in Figure 9. Further, on the basis of the data recorded to date, it is clear that there are now no inherent problems with the fabrication of MAMA detectors with pixel dimensions as small as $12 \times 12 \text{ microns}^2$. Refinements to the photocathode structures are now being investigated to improve the quantum efficiencies at ultraviolet and visible wavelengths and to extend the response into the near infrared. It is also clear that the current MCP structure and electronics technology will permit significant increases in the dynamic range with only relatively small increases in the total power requirements. The performance goals for these large-format arrays are sum-marized in Table 4 and compared with the present measured data.
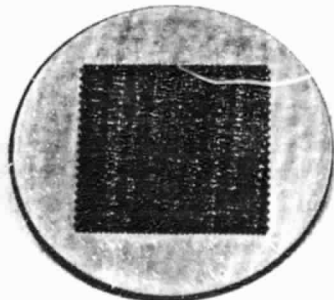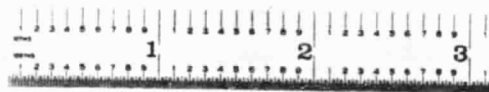
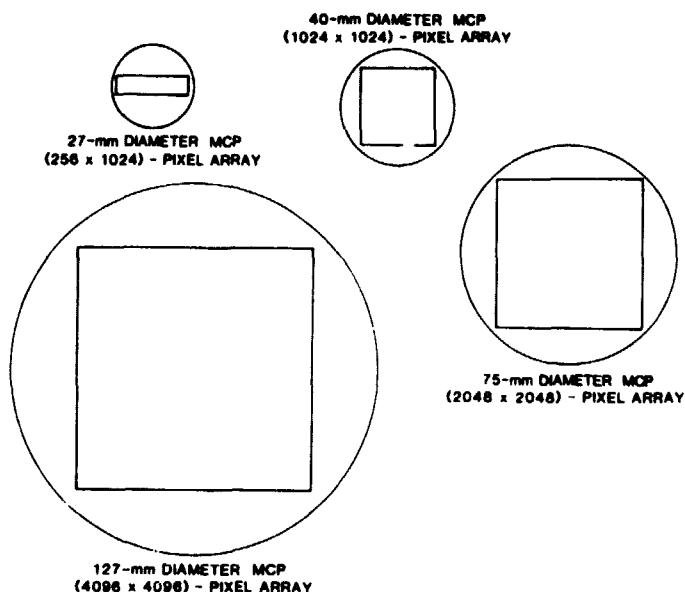Figure 8. 40-mm-format, curved-channel MCP with active area of $27 \times 27 \text{ mm}^2$.

Figure 9. Current and future MAMA detector formats.

Table 4. Summary of MAMA Performance Characteristics

	Achieved	Goal
MCP Active Area	40 mm diameter	127 mm diameter
Anode Array Format	256 x 1024	1024 x 1024 2048 x 2048 4096 x 4096
Spatial Resolution	25 microns (FWHM) (Rate Independent)	12 microns (FWHM) (Rate Independent)
Wavelength Range	< 3000 to 8500 Å	< 3000 to 9500 Å
Peak Quantum Efficiency (Ultraviolet and Visible Wavelengths)	$\sim$ 15 – 20%	> 30%
Pulse-Counting Detective Quantum Efficiency	65-80% of Q.E.	> 85% of Q.E.
Flat Field Uniformity	< 25% Peak-to-Peak	< 5% Peak-to-Peak

Defect Levels:
  Anode Array
  MCP Bright Spots
  MCP Dark Spots
	Zero
	Zero
	5 – 10
		Zero
		Zero
		< 5

Spatial Linearity	$\pm$5 microns over 26 mm	$\pm$5 microns over 90 mm

Maximum Count Rate (10% loss of DQE)
  Per pixel (25 x 25 microns^2)
  Per array
	> 100 cs^{-1} (random)
	10^6 cs^{-1} (random)
		$\sim$ 1000 cs^{-1} (random)
		10^7 cs^{-1} (random)

Lifetime	> 2.5 x 10^{11} counts mm^{-2} (25-micron pore size at 10^6 gain)	> 10^{13} counts mm^{-2}
Operating Temperature Range	+30 to –30°C	+30 to –30°C
Total System Power (does not include cooling)	< 30 W	< 60 W

Acknowledgements

References

1. Timothy, J. G., and R. L. Bybee, "Multi-Anode Microchannel Array Detectors for Space Shuttle Imaging Applications," SPIE Shuttle Pointing of Electro-Optical Experiments, Vol. 265, p. 93. 1981.
2. Timothy, J. G., and R. L. Bybee, "Multi-Anode Microchannel Arrays: New Detectors for Imaging and Spectroscopy in Space," AIAA 21st Aerospace Sciences Meeting, Vol. AIAA-83-0105, Reno, Nevada. 1983.
3. Timothy, J. G., "Optical Detectors for Spectroscopy," Pub. Astron. Soc. Pacific, Vol. 95, p. 810. 1983.
4. Litton Electron Devices, South 52nd Street, Tempe, Arizona 85281
5. Galileo Electro-Optics Corporation, Galileo Park, Sturbridge, Massachusetts 01518
6. Ball Aerospace Systems Division, P. O. Box 1062, Boulder, Colorado 80306-1062
7. Timothy, J. G., C. L. Joseph, and S. C. Wolff, "High Resolution Spectroscopy with the Multi-Anode Microchannel Array Detector System," SPIE Instrumentation in Astronomy IV, Vol. 331, p. 301. 1982.

ELECTRONIC READOUT SYSTEMS FOR MICROCHANNEL PLATES

J. Gethyn Timothy
Center for Space Science and Astrophysics, ERL 315
Stanford University
Stanford, California 94305

Abstract

The modes of operation of position-sensitive electronic readout systems for use with high-gain microchannel plates are described and their performance characteristics compared and contrasted.

Introduction

The microchannel plate (MCP) is an electron multiplier with a two-dimensional imaging capability. When coupled to a semi-transparent photocathode, the MCP forms a compact image intensifier which is widely used for night vision imaging applications. Alternatively, the MCP can be used in an open-structure configuration to detect high energy photons at extreme ultraviolet (EUV) and soft x-ray wavelengths or to directly detect charged particles.

The recent development of MCPs which can be operated at high gain in the pulse-counting mode has made it possible to develop position-sensitive electronic systems which can directly detect the charge pulse from the MCP. These digital imaging systems have a large number of applications in astrophysics, plasma physics, and high-energy nuclear physics. The operating characteristics of the different systems which are currently in use or under development and their requirements on the performance characteristics of the high-gain MCPs are described in this paper. Alternative readout techniques in which the electron cloud from the MCP is converted to visible-light photons by a phosphor and detected by photosensitive arrays, such as described by Hartig et al.[1] and Weistrop et al.[2], will not be reviewed here.

High-Gain Microchannel Plates (MCPs)

The MCP operates in an identical manner to that of the conventional channel electron multiplier (CEM) which consists of a semi-conducting glass channel having an internal diameter of a few millimeters and a length-to-diameter ratio of the order of 100:1. In operation, a potential of about 2000 V is applied along the length of the channel when the CEM is in a high-vacuum enclosure. An electron released from the wall of the channel at the input by the impact of either a photon or a charged particle is accelerated along the channel axis and drifts across to strike the wall with sufficient energy to release secondary electrons (see Figure 1a). The process is repeated throughout the length of the channel, and the output charge pulse, normally containing 10^6 to 10^8 electrons, is collected at the anode. The channel of a high-gain CEM is curved to inhibit the acceleration of positive ions produced by the impact of electrons with residual gas molecules towards the cathode where they can initiate secondary avalanches producing a noisy and unstable device.

At high gain the amplitude of the output pulse is clipped by the effects of space charge within the channel, and the output pulse-height distribution has the saturated form shown in Figure 1b. The resolution of the output pulse-height distribution can be defined as

$$R = \Delta G / \bar{G}$$

where ΔG equals the full width at the half height of the distribution and $\bar{G}$ equals the modal gain value. Resolutions of the order of 30 to 50% are typically obtained.
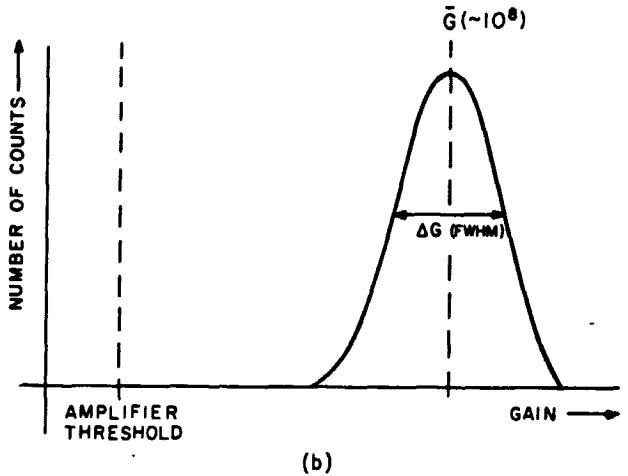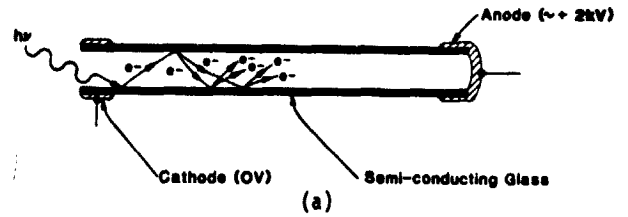

Figure 1. The Channel Electron Multiplier (CEM).
a. Mode of operation.
b. Form of output pulse-height distribution.

Since the performance of the CEM depends principally on the length-to-diameter ratio of the channel and on the applied potential and not on the absolute physical dimensions, the CEM can be reduced to a size set by the limitations of glass fiber technology (typical channel diameters of the order 8 to 20 microns). Large numbers of these small channels can then be assembled together in a billet using the techniques described by Wiza[3] to produce a microchannel plate (MCP) which consists of a glass disk composed of several million channels each of which can act as an independent multiplier.

The MCP is thus an electron multiplier with a two-dimensional imaging capability. Until recently, MCPs could only be fabricated with straight channels, and a single MCP was susceptible to ion feedback instabilities when operated at high gain. However, MCPs can be obtained with the channels set at any bias angle with respect to the face of the plate in tne range from 0 to 60°, and a multiplier can be constructed from two or more MCPs with suitable bias angles and plate orientations so that positive ions are trapped at the interfaces between the plates as shown in Figure 2. The total voltage across the MCPs can then be increased to the level at which a stable high gain and a saturated output pulse-height distribution are obtained.

Generally, the output pulse-height distributions for two or three cascaded MCPs in "chevron" or "Z-plate" configurations are inferior to those of conventional CEMs; although tight pulse-height distributions (resolutions of the order of 40 to 60%) have been reported for "chevron" configurations using MCPs with
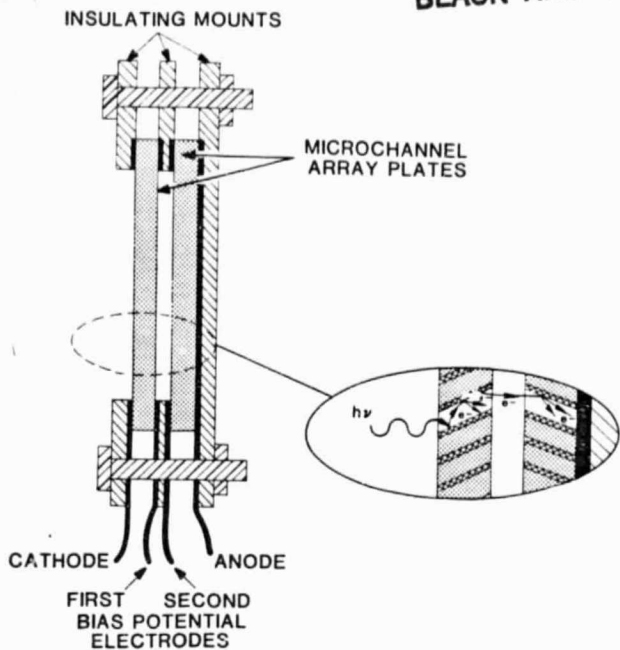
1

Figure 2. Straight-channel MCPs in a "chevron" config-
uration for high-gain operation.

channel length-to-diameter ratios of 80:1 (see, for
example, Siegmund et al.[4]). The recent fabrication of
MCPs in which the channels are curved to inhibit ion
feedback in an identical manner to that employed in a
CEM (see Figure 3) has accordingly significantly
improved the performance characteristics of a single
MCP. Gains of greater than 10^6 electrons pulse^{-1},
resolutions of the output pulse-height distribution of
40% or better (see Figure 4), and lifetimes in excess
of 2×10^{11} counts mm^{-2} have been obtained with MCPs
having C-configuration channels.[5] The diameters of the
channels in currently available MCPs range from 8 to 25
microns, and the high-gain MCP accordingly has the
potential to provide a very high spatial resolution.

Electronic Readout Systems

In the simplest type of position-sensitive elec-
tronic readout system, the spatial resolution is
defined solely by the geometry of the electrodes in the
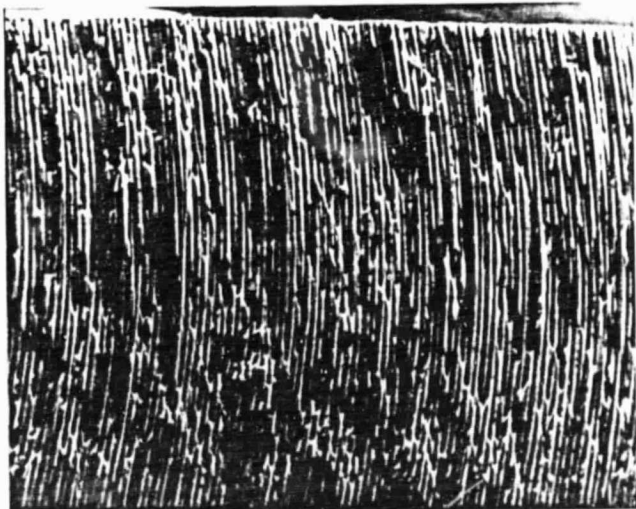anode array. Each anode, i.e. pixel, is connected to an

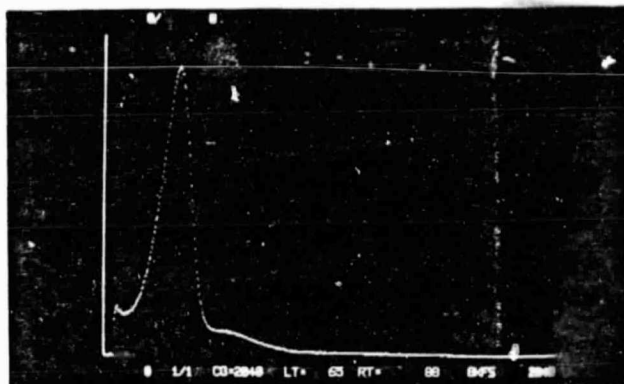

Figure 3. Section of curved-channel MCP.

Figure 4. Output pulse-height distribution for a
curved-channel MCP with 25-micron-diameter
channels. Modal gain 1.3×10^6.
Resolution 40% (FWHM).

amplifier and counting circuit. This is the discrete-
anode readout system (see Figure 5). Two examples of
this type of readout array fabricated by the author and
his associates[6] are shown in Figure 6. The first,
shown in Figure 6a, is a (10 x 10)-pixel array with
pixel dimensions of 1.2 x 1.2 mm^2 which is being used
as a simple imaging system for photometric studies and
for tracking applications. The second array, shown in
Figure 6b, is a 160-pixel linear array designed for use
as a high-dynamic-range spectroscopic detector. The
discrete anode system provides distortion-free imaging
and a high dynamic range and has great flexibility in
providing configurations that are optimized for spe-
cialized needs. However, the system has a limitation
in that the total number of pixels is restricted to
about 500 by currently available connector and elec-
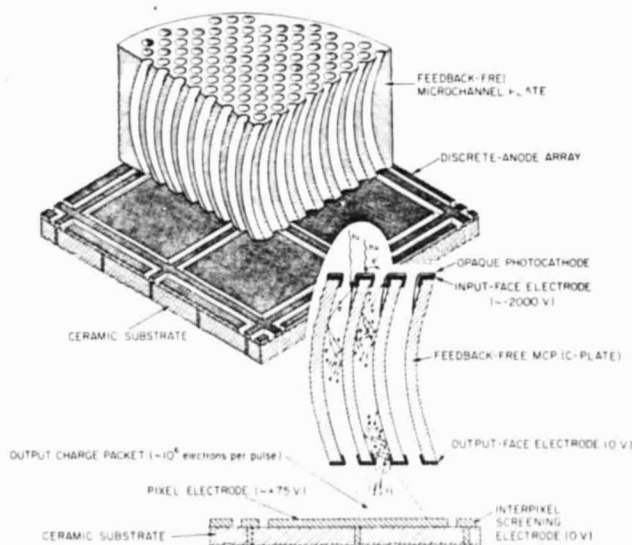tronics technologies.

Figure 5. Schematic of discrete-anode MCP detector.

A number of electronic readout systems have been
developed which employ a centroiding technique to iden-
tify the location of the charge pulse. The simplest of
these systems employs a resistive anode to locate the
event by means of charge division[7] or rise-time[8] encod-
ing techniques. The block diagram of a one-dimensional
resistive anode encoder using rise-time discrimination[3]
is shown in Figure 7. In a one-dimensional array, an
amplifier is connected to each end of a resistive
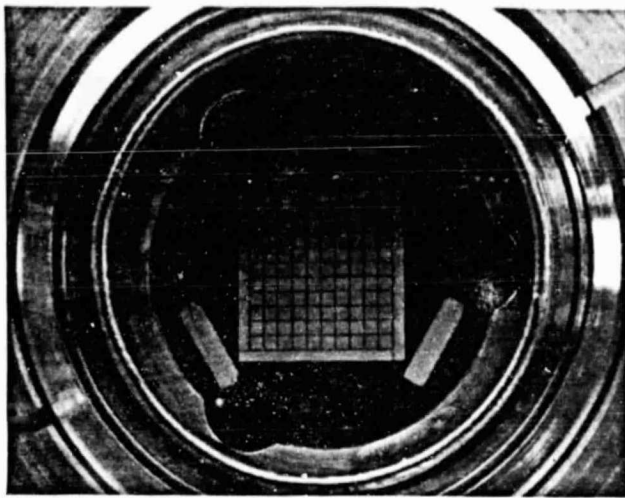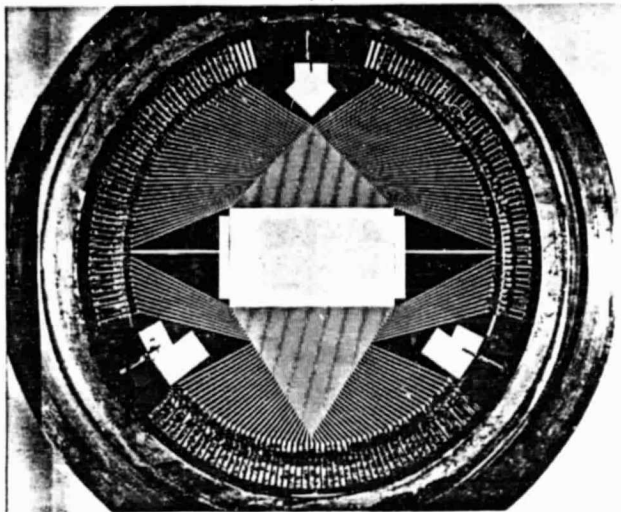
Figure 6. Discrete anode arrays.
a. (10 x 10)-pixel array with pixel dimensions of 1.2 x 1.2 mm^2.
b. (1 x 160)-pixel array with pixel dimensions of 8 mm x 100 microns.

Figure 7. Block diagram of a one-dimensional, resistive-anode encoder employing rise-time discrimination (from Wiza[3]).

sheet. The output charge pulse from the MCP will be divided between the two amplifiers in proportion to the distance of the pulse from the ends of the sheet. The spatial location can accordingly be determined by ratioing the charge detected by the two amplifiers or by measuring the differences in the rise times of the two charge pulses. A two-dimensional, resistive anode array can be constructed with four amplifiers, one at each corner of the sheet. In this case the position is determined in two dimensions from the ratios of the charge detected by opposite pairs of amplifiers. One-dimensional resistive anode arrays give good spatial linearity; but two-dimensional resistive anode arrays require low resistivity borders to overcome significant image distortion caused by charge reflection effects.[9]

This simple system has a number of limitations. First, the spatial resolution is dependent on the gain of the MCP; and for the best spatial resolutions, the resistive anode encoder requires gains in excess of 10^7 electrons pulse^{-1} dictating the use of "chevron" or "Z-plate" MCP stacks in which the charge cloud is allowed to spread over a number of channels. The best resolution obtained to date, of the order of
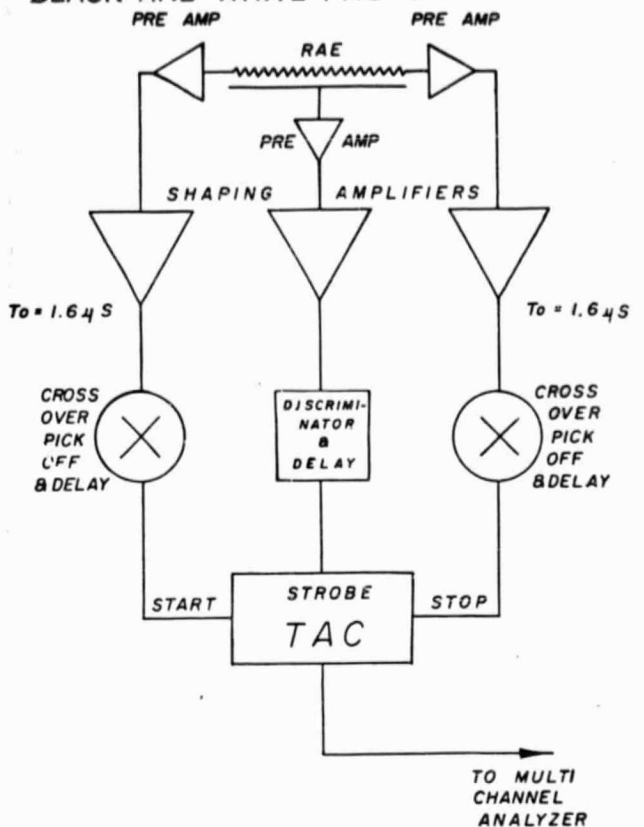
40 microns, requires a stack of five MCPs[10,11] to produce a gain approaching 10^8 electrons pulse^{-1}. Second, the spatial resolution begins to degrade because of pulse pileup at signal levels in excess of about 10^4 counts s^{-1} (random). At high count rates the coincident arrival of pulses is interpreted by the readout electronics as a single event midway between the two simultaneous events (see, for example, Mertz et al.[12]). This causes a false image to be formed between bright areas in the detected image.

A more complex version of the resistive anode encoder which uses discrete anode wires resistively coupled in sets is the High-Resolution Imager (HRI)[13] developed by the Smithsonian Astrophysical Observatory for use as an x-ray detector on the Einstein mission and later as an optical detector (Photicon).[14] The readout technique for the HRI is shown schematically in Figure 8. An amplifier is connected to every eighth wire with a total of 34 amplifiers used for the two-dimensional system. The amplifiers are combined into three groups, and the fine position of the centroid is determined from the division of charge among the three groups by using a cyclic algorithm of the form (A-C)/(A+B+C). The coarse position is determined by the rank of the amplifiers. The accuracy of determining the centroid is of the order of 15-30 microns (1σ fit).

The ultimate spatial resolution in the resistive anode systems will, however, be limited by thermal noise[7] and accordingly a number of centroiding systems utilizing conducting electrodes have been developed. The simplest is the quadrant anode shown in Figure 9. In this system, the position of the charge pulse is determined by simply ratioing the charge collected on the four anodes.[15,16] This extremely simple system has
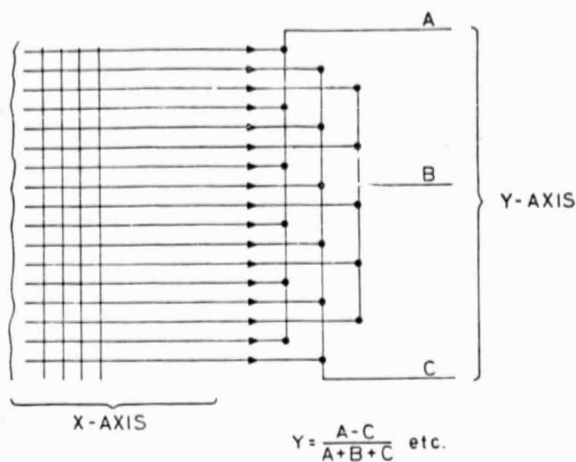
Figure 8. Schematic of HRI and Photicon readout system (from Kellogg et al. [13]).
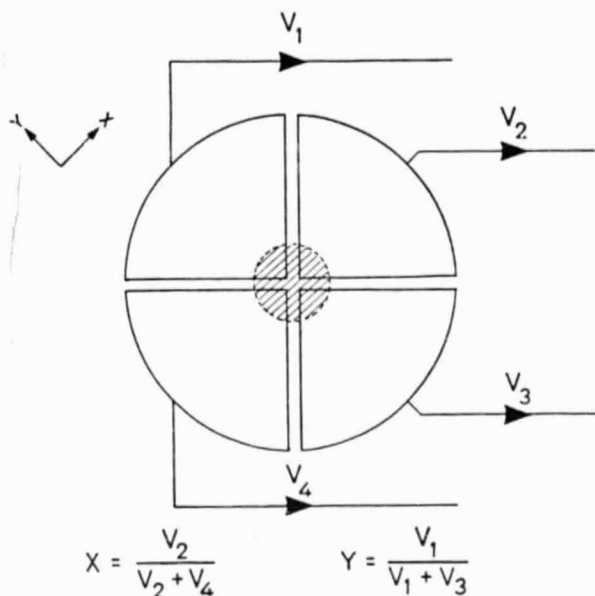
$$Y = \frac{A-C}{A+B+C} \text{ etc.}$$

$$X = \frac{V_2}{V_2 + V_4} \qquad Y = \frac{V_1}{V_1 + V_3}$$

Figure 9. Schematic of quadrant anode readout system (from Lampton and Malina[15]).

$$X = \frac{C}{C+D}$$
$$Y = \frac{A}{A+B}$$

Figure 10. Schematic of four-electrode wedge-and-strip readout array (from Martin et al.[18]).

a very limited active area determined by the diameter of the charge pulse arriving at the electrode structure, and image distortions increase rapidly off-axis. A more complex system of this type using a number of electrodes in a hexagonal structure to improve the linearity over a larger distance has been described by Gruntman,[17] although no details on the performance characteristics have so far been presented.

Probably the most effective of the centroiding systems in use today is the wedge-and-strip array[18] developed by a group at the University of California, Berkeley. A schematic of a typical wedge-and-strip array configuration is shown in Figure 10. In this array, charge is collected on a number of discrete conducting electrodes, but positional information is once again determined by the ratio of the charge collected on the different electrodes. In the array shown in Figure 10, the coordinates of the event in the horizontal (X-axis) are determined by the ratio of the charge collected on electrodes C and D, and in the vertical (Y-axis) by the ratio of the charge collected
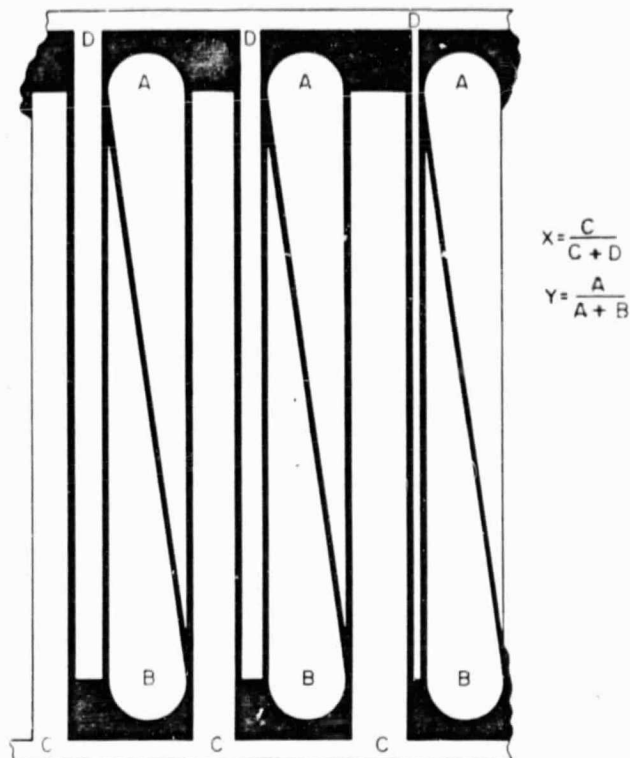
on the electrodes A and B. Two-dimensional wedge-and-strip arrays can be constructed with only three electrodes.[4] Spatial resolutions of the order of 40 microns have been obtained with MCP gains in excess of 10^7 electrons pulse^{-1}.

The most complex of the centroiding readout systems is the Codacon which is currently under development at the University of Colorado.[19] The Codacon anode array configuration is shown in Figure 11. Charge collected on the pixel electrode ("charge spreader") is capacitatively coupled into the code tracks to generate the address of the event location. This binary encoding technique requires 20 tracks and 10 differential amplifiers for a 1024-pixel array. The capacitative coupling of the charge pulse to the output electrodes results in a lower signal-to-noise than for an equivalent all-conducting electrode structure. More seriously, the readout array is extremely difficult to
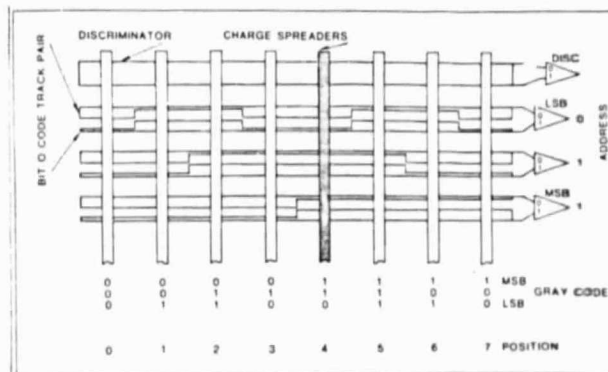

Figure 11. Schematic of eight-channel Codacon readout array (from McClintock et al.[19]).

4

fabricate since it requires a "leaky" dielectric to dissipate the charge from the pixel electrodes. If the resistivity of the dielectric is too high, the pixel electrodes will charge and effectively shut down the readout system. Only limited performance data for the Codacon have been made available to date.

A readout system which is designed to eliminate the high-gain requirements and the dynamic range limitations of centroiding systems and which uses a precision array of electrodes to collect the charge pulse is currently under development by the author in collaboration with Ball Aerospace Systems Division (BASD). The multi-layer, coincidence-anode, Multi-Anode Microchannel Array[6,20] (MAMA) (see Figure 12) employs two sets of anodes insulated from each other but exposed to the output face of the MCP. The output charge cloud from the MCP divides between the two sets of anodes at the position where the event occurs allowing the spatial location to be identified by the coincident arrival of pulses on the appropriate pair of anodes. Photometric data from $a \times b$ pixels can then be read out with a total of a + b amplifier and discriminator circuits. As shown in Figure 13a, a (1 x 1024)-pixel linear array, for example, has a total of 32 x 32 pixels and requires 32 + 32 amplifier and discriminator circuits. Two-dimensional arrays can be constructed from two identical coincidence anode arrays arranged vertically above each other and oriented orthogonally. As shown in Figure 13b, a (1024 x 1024)-pixel array fabricated in this manner employs coincidence detection in the two axes and requires only a total of 128 amplifier and discriminator circuits.
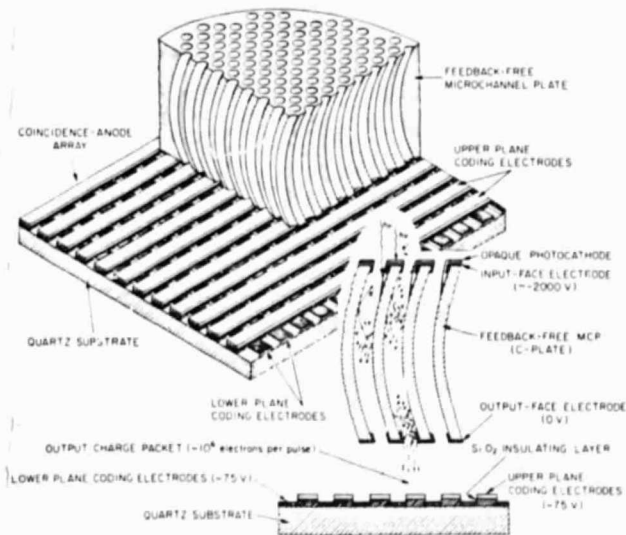

Figure 12. Schematic of multi-layer, coincidence-anode readout array (from Timothy[20]).

The technical problem in the fabrication of these multi-layer arrays is the need to expose the lower-layer electrodes to the low energy (order of 30 V) electrons from the MCP which cannot penetrate an insulating layer. This is accomplished by etching away the silicon dioxide insulating layer between the two sets of electrodes in the interstices between the upper layer electrodes. The largest format coincidence anode arrays in operation today have formats of 256 x 1024 pixels and spatial resolutions of 25 x 25 microns² (FWHM).

Summary of Performance Characteristics

The key performance characteristics of the different electronic readout systems are listed in Table 1. On the basis of the performance data
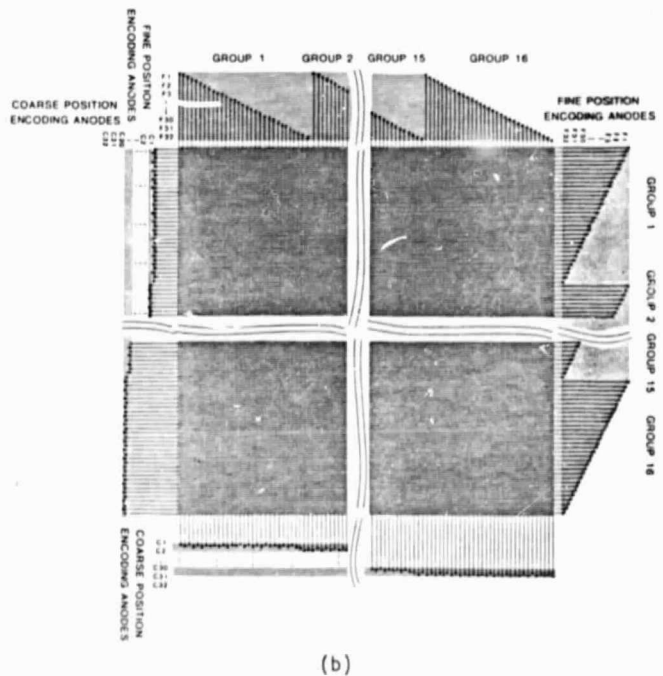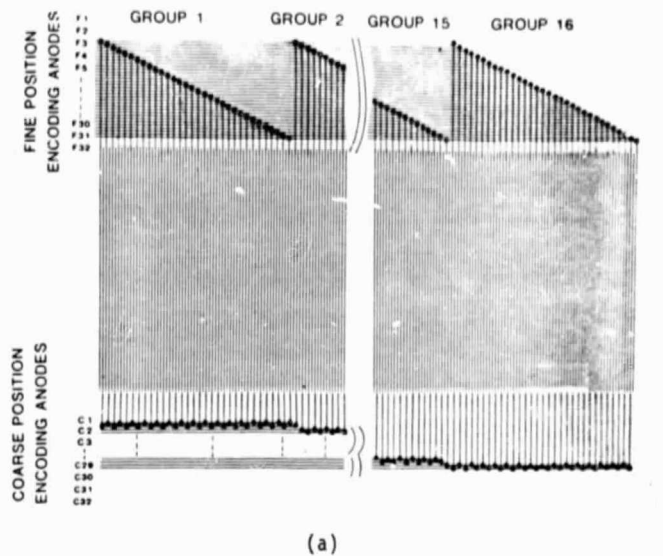

(a)

(b)

Figure 13. Configurations of coincidence-anode MAMA readout arrays.
a. (1 x 1024)-pixel linear array.
b. (1024 x 1024)-pixel imaging array.

available to date, it would appear that the readout systems using only conducting electrodes offer the best performance characteristics; specifically, the discrete-anode arrays for applications requiring a high dynamic range and a limited number of pixels, the wedge-and-strip arrays for imaging applications requiring moderate spatial resolution and dynamic range, and the coincidence-anode arrays for imaging applications requiring high spatial resolution and dynamic range.

Table 1. ELECTRONIC READOUT SYSTEMS FOR MCPS

Type	Format	Pixel Dimensions (microns²)	Active Area (mm²)	Point Spread Function (FWHM) (microns)	Number of Amplifiers	Charge Division Factor	Temporal Resolution	Count Rate for 10% Coincidence Loss (counts s⁻¹) Single Pixel	Array	Comments	References
Discrete Anode	10 x 10 / 1 x 160	1200 x 1200 / 8000 x 100	12 x 12 / 8 x 16	1200 / 100	100 / 160	1 / 1	100 ns / 100 ns	> 1.5 x 10⁹ / > 10⁶	> 1.5 x 10⁷ / > 1.5 x 10⁷	Very high dynamic range. Distortion-free imaging. Limited number of pixels.	[6]
Resistive Anode	~800 x 800	~25 x 25	26 ∅	~40	4	1600	~2 μs	10²	8 x 10⁴	Resolution limited by thermal noise. False imaging at high count rates. Edge distortions with two-dimensional arrays. Resolution is gain and count-rate dependent. Requires very high gain.	[10] [11] [12]
Photicon	~2600 x 2600	~10 x 10	26 x 26	~30	34	320	~1 μs	?	10⁴	Higher spatial resolution than resistive anode. Different spatial linearities in different sectors of array. Artifacts at sector interfaces.	[13] [14]
Quadrant Anode	100 x 100	~10 x 10	1 x 1	~18	4	200	~1 μs	?	10⁵	Very limited active area. Image distortions increase rapidly off-axis. Susceptible to strong magnetic fields.	[15] [16]
Wedge and Strip	~1000 x 1000	~40 x 40	40 ∅	~40	3	2000	< 10 μs	10²	> 10⁴	Very low image distortion. Requires high gain. Resolution is gain and count-rate dependent. Possibility of some false images at high count rates. Susceptible to strong magnetic fields.	[18] [4]
Codacon	1 x 1024	1200 x 25	13 x 26	~50 ?	10 (differential)	11	< 1 μs ?	?	?	Poor signal-to-noise because of capacitative coupling to output electrodes. Dynamic range limited by resistivity of "leaky dielectric". High-resolution imaging in two dimensions not yet demonstrated.	[19]
Coincidence Anode MAMA	1 x 1024 / 16 x 1024 / 256 x 1024	6500 x 25 / 400 x 25 / 25 x 25	6.5 x 26 / 6.5 x 26 / 6.5 x 26	25 / 25 / 25	64 / 80 / 96	3 / 4 / 6	100 ns / 100 ns / 170 ns	~10⁶ / ~6 x 10³ / ~4 x 10²	10⁶ / 10⁶ / 10⁶	Image quality independent of gain or signal level. Requires moderate gain. Distortion-free imaging. Maximum count rate limited by pulse-pair resolution of electronics.	[6] [20]

References

[1] G. F. Hartig, H. W. Moos, R. Pembroke, and C. Bowers, SPIE Instrumentation in Astronomy IV, vol. 331, p. 45, 1982.

[2] D. Weistrop, J. T. Williams, A. Boggess, K. L. Hallam, D. A. Klinglesmith III, and R. W. O'Connell, AAS Photo-Bulletin, no. 35, p. 3, 1984.

[3] J. L. Wiza, Nuclear Instruments and Methods, vol. 162, p. 587, 1979.

[4] O. H. W. Siegmund, S. Clothier, J. Thornton, J. Lemen, R. Harper, I. M. Mason, and J. L. Culhane, IEEE Trans. Nucl. Sci. NS-30, no. 1, p. 503, 1983.

[5] J. G. Timothy, Rev. Sci. Instrum., vol. 52, p. 1131, 1981.

[6] J. G. Timothy and R. L. Bybee, SPIE Shuttle Pointing of Electro-Optical Experiments, vol. 265, p. 93, 1981.

[7] M. Lampton and F. Paresce, Rev. Sci. Instrum., vol. 45, p. 1098, 1974.

[8] W. Parkes, K. D. Evans, and E. Mathieson, Nuclear Instruments and Methods, vol. 121, p. 151, 1974.

[9] M. Lampton and C. W. Carlson, Rev. Sci. Instrum., vol. 50, p. 1093, 1979.

[10] C. Firmani, E. Ruiz, C. W. Carbon, M. Lampton, and F. Paresce, Rev. Sci. Instrum., vol. 53, p. 570, 1982.

[11] C. Firmani, L. Gutierrez, E. Ruiz, G. F. Bisiacchi, L. Salas, F. Paresce, C. W. Carlson, and M. Lampton, Astronomy and Astrophysics, vol. 134, p. 251, 1984.

[12] L. N. Mertz, T. D. Tarbell, and A. M. Title, Applied Optics, vol. 21, p. 628, 1982.

[13] E. Kellogg, P. Henry, S. Murray, L. Van Speybroeck, and P. Bjorkholm, Rev. Sci. Instrum., vol 47, p. 282, 1978.

[14] E. Kellogg, S. Murray, U. Briel, and D. Bardas, Rev. Sci. Instrum., vol. 48, p. 550, 1977.

[15] M. Lampton and R. F. Malina, Rev. Sci. Instrum., vol. 47, p. 1360, 1976.

[16] R. W. Wijnaendts van Resandt, H. C. den Harink, and J. Los, Journal of Physics E: Scientific Instruments, vol. 9, p. 503, 1976.

[17] M. A. Gruntman, in Instruments and Experimental Techniques (USSR), to be translated into English by Plenum Publishing Corp., 1984.

[18] C. Martin, P. Jelinsky, M. Lampton, R. F. Malina, and H. O. Anger, Rev. Sci. Instrum., vol. 52, p. 1067, 1981.

[19] W. E. McClintock, C. A. Barth, R. E. Steele, G. M. Lawrence, and J. G. Timothy, Applied Optics, vol. 21, p. 3071, 1982.

[20] J. G. Timothy, SPIE State-of-the-Art Imaging Arrays and Their Applications, in press, 1984.